



**HAL**  
open science

## Bandwidth Unlimited Polarization-Maintaining Metasurfaces

Q. Song, S. Khadir, S. Vézian, B. Damilano, P. D Mierry, S. Chenot, V.  
Brandli, Patrice Genevet

► **To cite this version:**

Q. Song, S. Khadir, S. Vézian, B. Damilano, P. D Mierry, et al.. Bandwidth Unlimited Polarization-Maintaining Metasurfaces. Science Advances , 2021, 7 (5), 10.1126/sciadv.abe1112 . hal-03582572

**HAL Id: hal-03582572**

**<https://hal.science/hal-03582572>**

Submitted on 21 Feb 2022

**HAL** is a multi-disciplinary open access archive for the deposit and dissemination of scientific research documents, whether they are published or not. The documents may come from teaching and research institutions in France or abroad, or from public or private research centers.

L'archive ouverte pluridisciplinaire **HAL**, est destinée au dépôt et à la diffusion de documents scientifiques de niveau recherche, publiés ou non, émanant des établissements d'enseignement et de recherche français ou étrangers, des laboratoires publics ou privés.

## FRONT MATTER

### Title

- Bandwidth Unlimited Polarization-Maintaining Metasurfaces.

### Authors

Q. Song, S. Khadir, S. Vézian, B. Damilano, P. D. Mierry, S. Chenot, V. Brandli, P. Genevet\*

### Affiliations

Université Cote d'Azur, CNRS, CRHEA, Rue Bernard Gregory, Sophia Antipolis 06560 Valbonne, France

### Abstract

Any arbitrary state of polarization of a light beam can be decomposed into a linear superposition of two orthogonal direction of the oscillations, each of which has a specific amplitude of the electric field. The dispersive nature of diffractive and refractive optical components generally affects these amplitudes significantly over a small wavelength range, tumbling the light polarization properties. Although recent works suggest the realization of broadband nanophotonic interfaces that can mitigate frequency dispersion, their usage for arbitrary polarization control remains elusively chromatic. Here, we present a general method to address broadband full-polarization properties of diffracted fields using an original superposition of circular polarization beams transmitted through metasurfaces. This concept of polarization-maintaining metasurfaces is applied to realize complex broadband wavefront shaping, including beam deflectors and white-light holograms. Eliminating the chromatic dispersion and dispersive polarization response of conventional diffractive elements lead to broadband polarization-maintaining devices of interest for applications in polarization imaging, broadband-polarimetry, augmented/virtual reality imaging, full color display, etc.

## MAIN TEXT

### Introduction

Polarization, one of the key parameters of electromagnetic wave, plays a significant role in many areas, such as 3D stereoscopic displays, quantum computation, chemical sensing, etc. Conventional generation method of arbitrary polarization involves bulky optical components combining polarizers and waveplates. In recent years, metasurfaces with optically thin thickness have been proposed by locally designing subwavelength structures to control all of the parameters of the electromagnetic wave, such as phase (1, 2), frequency (3), amplitude (4), propagation direction (5, 6), and polarization (7–10), leading to various applications, including lenses (11), cloaking (12), sensing (13, 14), information security (15), etc. The manipulation of polarization state of light using metasurfaces usually relies on designing the structural properties of anisotropic (16) and chiral nanostructures (17). The superposition of two orthogonal polarizations has been proposed to generate versatile output polarization, simply by controlling the offset between the two polarization components (18, 19). However, to generate full arbitrary polarization, the amplitude difference of the two polarization components has to be precisely controlled

48 (20). Amplitude control has generally been performed through the nanostructure  
49 geometric sizes, at the expense of introducing a huge dispersion of the amplitude response,  
50 compromising the device broadband operation, as schematically shown in Fig. 1A and 1B.

51 Here, we propose a general method to maintain the full polarization state of diffracted  
52 signal, essentially over an unlimited wavelength range, by using appropriate superposition  
53 of orthogonal circular polarization (CP) (see schematic in Fig.1C and 1D). We also prove  
54 that our approach is compatible with basic chromatic dispersion compensation using a  
55 simple metasurface doublet (see schematic in Fig.1E and 1F), thus demonstrating for the  
56 first time a broadband white-light holographic image with broadband polarization-  
57 maintaining performances. The control of polarization helicity, i.e. left CP (LCP) or right  
58 CP (RCP), and the direction of the scattered light are controlled through an arrangement of  
59 spatially oriented birefringent geometric-phase meta-structures. This peculiar method to  
60 address wavefront ranging from basic beam deflection to complex holographic field  
61 distribution (21–28), relies on replication and rotation of a unique nanostructure. In  
62 general, the intrinsic dispersive modal response of the nanostructure creates strong  
63 dispersive response, but in this contribution, we report an interesting superposition regime  
64 for which the dispersive contribution of the antenna does not comprehend the overall  
65 polarization response. The method consists in superposing: a) diffracted fields with the  
66 same handedness of CP to control the output light amplitude, essentially relying on simple  
67 interference condition and b) an additional phase retarded diffracted field oscillating on  
68 the opposite handedness, to access full polarization of the output light. **Previously, vectorial  
69 meta-hologram able to address the problem of polarization dependent image projection  
70 has been proposed, increasing the design degrees of freedom to enable polarization  
71 multiplexing (29–34).** A reflective meta-hologram based on diatomic metasurface has  
72 been proposed for the full polarized meta-hologram at oblique incidence (35, 36). Full  
73 polarized meta-hologram can also be realized by combining geometric phase and  
74 propagation phase, which suffers from narrow bandwidth (37–39). In this manuscript, we  
75 applied our concept of polarization-maintaining metasurfaces to encode complex phase  
76 profiles with geometric phase gradient metasurfaces and experimentally demonstrated  
77 arbitrary polarization holographic images with broadband characteristics.

## Results

### Design method of polarization-maintaining metasurfaces

Our general concept of the proposed broadband-polarization addressing metasurfaces is illustrated in Fig. 1C and compared with respect to the dispersive design in Fig. 1A. A 1  $\mu\text{m}$ -thin GaN film on the  $x$ - $y$  plane is etched to form rectangular pillars suitably disposed and oriented to acquire the desired geometric phase and shape a given incident CP into a deflected beam with opposite helicity. The excitation input light beam propagating along the  $-z$  direction is chosen to be linearly polarized in the  $x$ -direction, and can thus be decomposed into two CP beams with equal amplitude and phase. Noted that the incident light can be arbitrary polarization except for two pure CP beams (see more details in Supplementary Note 3 and Note 4). As considered in the literature (22), a single PB phase gradient array is able to direct the two incident CP beams into deflected beams with opposite helicity accordingly to their incident polarization spin. In this first example Fig. 1A, the dispersive case, the first meta-structures line in the bottom of the metasurface is arranged counterclockwise with an orientation angle increment of  $\delta_d$  to deflect the incident RCP into an LCP beam propagating at an angle of  $\theta_{ld} = \arcsin(\lambda\delta_d / \pi P)$ , where  $\lambda$  is the operating wavelength and  $P$  is the period of the meta-structures. The complex transmission of LCP beam is  $a_1(\lambda)e^{i\varphi_1(\lambda)}e^{-i2\delta_L}$  (see Supplementary Eq. S3) with starting rotation angle (SOA) of  $\delta_L$ , where the conversion efficiency  $a_1(\lambda)$  and propagation phase  $\varphi_1(\lambda)$  are usually dispersive and related to the size of the bottom meta-structures, while the geometric phase  $-2\delta_L$  is only related to the rotation angle of the meta-structures. The additional meta-structures disposed in the top line of the metasurface are arranged clockwise with the same angle increment of  $\delta_d$  to convert the LCP into an RCP beam propagating at the same angle of  $\theta_{ld}$ . The transmitted RCP has the complex amplitude of  $a_2(\lambda)e^{i\varphi_2(\lambda)}e^{-i2\delta_R}$  according to Supplementary Eq. S3 with SOA of  $\delta_R$ , where  $a_2(\lambda)$  and  $\varphi_2(\lambda)$  are related to the size of the top meta-structures. Therefore, the output SoP can be described as,

$$|n_{LR}\rangle = a_1(\lambda)e^{i\varphi_1(\lambda)}e^{-i2\delta_L}|+\rangle + a_2(\lambda)e^{i\varphi_2(\lambda)}e^{i2\delta_R}|-\rangle \quad (1)$$

The ellipticity becomes  $\chi = \frac{1}{2} \arcsin \frac{a_2(\lambda)^2 - a_1(\lambda)^2}{a_2(\lambda)^2 + a_1(\lambda)^2}$  and the azimuth angle is

$\psi = \frac{\varphi_2(\lambda) - \varphi_1(\lambda)}{2} + \delta_R + \delta_L$ . Since  $a_{1,2}(\lambda)$  and  $\varphi_{1,2}(\lambda)$  are usually dispersive, the output polarization is related to the wavelength as shown in the schematic of Fig. 1B.

To address this problem, we propose an interesting superposition using three lines of phase gradient metasurface as shown in Fig. 1C. The broadband polarization-maintaining design consists of controlling the diffraction of one LCP and two RCP with SOA of  $\delta_{L1}$ ,  $\delta_{R1}$  and  $\delta_{R2}$ . The key idea is to homogenize the dispersion effect utilizing a unique meta-

structure, i.e. only one nanopillar with uniform size, for all lines, so that all transmitted LCP and RCP beams share the same conversion efficiency  $a(\lambda)$  and propagation phase  $\varphi(\lambda)$ . According to Supplementary Eq. S3, the output polarization can be written as,

$$\begin{aligned} |n_{LRR}\rangle &= a(\lambda)e^{i\varphi(\lambda)}e^{-i2\delta_{L1}}|+\rangle + a(\lambda)e^{i\varphi(\lambda)}e^{i2\delta_{R1}}|-\rangle + a(\lambda)e^{i\varphi(\lambda)}e^{i2\delta_{R2}}|-\rangle \\ &= a(\lambda)e^{i\varphi(\lambda)}\left(e^{-i2\delta_{L1}}|+\rangle + e^{i2\delta_{R1}}|-\rangle + e^{i2\delta_{R2}}|-\rangle\right) \end{aligned} \quad (2)$$

It can be seen that the dispersive term  $a(\lambda)e^{i\varphi(\lambda)}$  factorizes, leading to the generated polarization only related to the rotation angle of  $\delta_{L1}$ ,  $\delta_{R1}$  and  $\delta_{R2}$ , yielding to a nondispersive polarization behavior with unlimited bandwidth as shown in the schematic of Fig. 1D. It should be noted that the deflection efficiency, which depends upon the polarization conversion efficiency of the building block, changes as a function of the incident wavelength. Further efforts in designing broadband half-waveplate nanostructure could be realized to improve the device performance over much larger spectral range. Since the diffracted angles of the converted light beam  $\theta_{td}$  (Supplementary Eq. S7) of both the dispersive and nondispersive polarization design are angular dispersive, a metasurface-doublet is designed to eliminate the angular dispersion as shown in Fig. 1E and 1F (see more details in Supplementary Note 5).

### Simulated results and dispersion analysis

We performed the numerical simulation of realistic nanostructures using full-wave finite-difference time-domain (FDTD). The meta-structure consists of GaN nanopillars on a sapphire substrate as shown in Fig. 2A and 2B. The period of the meta-structure is chosen to avoid spurious diffraction effects in the substrate as  $P = 300$  nm, the thickness of the GaN nanopillar is  $h = 1$   $\mu\text{m}$  (see more simulated results in Supplementary fig. S5). To better explain the difference between our proposed broadband polarization-addressing method using a unique nanostructure size with respect to the conventional dual-nanostructure reconstruction method, i.e. dispersive superposition obtained with different nanostructure sizes (20), we carried out numerical simulation for both methods as shown in Fig. 2. **We first numerically calculated the polarization conversion efficiency  $a(\lambda)$  (red and black lines) and propagation phase  $\varphi(\lambda)$  (blue and green lines) with two different size of GaN nanopillars as shown in Fig. 2C.** As expected, one can see that both  $a(\lambda)$  and  $\varphi(\lambda)$  are highly dependent on the size of the nanostructures. Thereafter, we simulated the azimuth angle and ellipticity angle of the output polarization as a function of the incident wavelength for both cases (Fig. 2D and 2F for dispersive case, calculated from Eq. 1, and polarization-maintaining case, calculated from Eq. 2, respectively) and the corresponding SoP on Poincaré sphere (Fig. 2E and 2G for dispersive and polarization-maintaining, respectively). The dispersive superposition based on two nanostructures with different sizes ( $L_{u1} = 170$  nm,  $L_{v1} = 70$  nm,  $\delta_L = 0^\circ$  for the bottom line and  $L_{u2} = 220$  nm,  $L_{v2} = 120$  nm,  $\delta_R = 0^\circ$  for the top line), exhibits strong wavelength dependent SoP (Fig. 2E), since  $a_{1,2}(\lambda)$  and  $\varphi_{1,2}(\lambda)$  have different dispersive responses according to Fig. 2C. While, our design with a uniform size of GaN nanopillars ( $L_{u2} = 220$  nm and  $L_{v2} = 120$  nm), oriented at different starting angles to address the chosen SoP eliminates dispersion even in the

156 presence of strong nanostructure dispersive response as shown in Fig. 2F and 2G with  $\delta_{LI}$   
 157  $= 0^\circ$ ,  $\delta_{R1} = 22.5^\circ$ , and  $\delta_{R2} = 22.5^\circ$ .

### 158 **Full-polarization generation**

160 Our superposition design not only addresses nondispersive polarization properties, but it  
 161 can also generate arbitrary and full-polarization with uniform size of the meta-structures.  
 162 To simplify the discussion, we propose to refer as LRR configuration (the design using  
 163 one LCP and two RCP) as shown in Fig. 3A, consisting of phase-gradient supercells with  
 164 controllable SOA of  $\delta_{L1}$ ,  $\delta_{R1}$ , and  $\delta_{R2}$ . Since the output polarization is related to the  
 165 relative phase difference between these three components, we fix  $\delta_{L1}$  as zero. According

166 to Eq. 2, the dispersive term  $a(\lambda)e^{i\varphi(\lambda)}$  factorizes, so the output SoP becomes  
 167  $|n_{LRR}\rangle = |+\rangle + (e^{i2\delta_{R1}} + e^{i2\delta_{R2}})|-\rangle = |+\rangle + a_-e^{i\delta_-}|-\rangle$ , where  $a_-$  and  $\delta_-$  are the amplitude  
 168 and phase of  $(e^{i2\delta_{R1}} + e^{i2\delta_{R2}})$ . Therefore, the ellipticity becomes  $\chi = \frac{1}{2} \arcsin \frac{a_-^2 - 1}{a_-^2 + 1}$  and

169 the azimuth angle is  $\psi = \frac{\delta_-}{2}$ . The ellipticity and azimuth angle as a function of  $\delta_{R2}$  are  
 170 shown in Fig. 3B and 3C, respectively. Since  $0 \leq a_- \leq 2$ , the ellipticity of the SoP has an  
 171 upper limit of  $\frac{1}{2} \arcsin \frac{3}{5}$  (i.e.,  $-\frac{\pi}{4} \leq \chi \leq \frac{1}{2} \arcsin \frac{3}{5}$ ). The corresponding Poincaré sphere  
 172 with  $\delta_{R1} = 0^\circ$ ,  $30^\circ$  and  $60^\circ$  are shown in Fig. 3D, 3E and 3F, respectively. A full  
 173 azimuth angle is realized as shown in Fig. 3G by controlling both  $\delta_{R1}$  and  $\delta_{R2}$  from  $0^\circ$   
 174 to  $180^\circ$ . Therefore, the generated SoPs cover the bottom sphere cap with  
 175  $-\frac{\pi}{4} \leq \chi \leq \frac{1}{2} \arcsin \frac{3}{5}$ . Likewise, the RLL configuration (one RCP and two LCP) shown in

176 Fig. 3H-3N can generate SoPs that cover the top sphere cap with  $-\frac{1}{2} \arcsin \frac{3}{5} \leq \chi \leq \frac{\pi}{4}$  as  
 177 shown in Fig. 3N. In this way, depending the choice of the desired diffracted state of  
 178 polarization, one could choose in the LRR and RLL configurations, leading to a full-  
 179 polarized and broadband properties of output light. It is noted that by using twofold  
 180 superposition with a uniform meta-structure, the dispersion term in Eq. 1 can also be  
 181 factorized, i.e.  $a_1(\lambda)e^{i\varphi_1(\lambda)} = a_2(\lambda)e^{i\varphi_2(\lambda)}$ , leading to a nondispersive property but only  
 182 for linear output polarization.

### 183 **Unlimited bandwidth polarization-maintaining meta-hologram**

185 As a proof of principle, we design four elliptical polarizations using the above mentioned  
 186 LRR and RLL configurations as shown in Fig. 4. The deflector is pixelated into pixel  
 187 array containing four meta-structures in  $x$  direction and three lines in  $y$  direction, per pixel.  
 188 By encoding the holographic phase profiles into pixelated metasurfaces, we are able to  
 189 generate holographic images with arbitrary polarization and broadband characteristics.  
 190 The details of the rotation angles and the corresponding ellipticities and azimuth angles  
 191 are shown in the Supplementary Table S1. We encode the holographic phase profiles to  
 192 exhibit four playing card suits of “Spade”, “Heart”, “Club” and “Diamond”. SEM images

of the fabricated metasurfaces with top and tilt view is shown in Fig. 4A and 4B. The measured holographic images illuminated with coherent laser source at  $\lambda = 600$  nm are shown in Fig. 4C (see more details of fabrication processes and measurement setup in Methods and Supplementary fig. S9, S11). The measured SoP is plotted as blue dots in the Poincaré sphere as shown in Fig. 4D, which agrees well with the designed SoP denoted by the red dots. The broadband response of the polarization is demonstrated in Fig. 5. The holographic images of “Spade” with the incident wavelength ranging from  $\lambda = 475$  nm to  $\lambda = 675$  nm are shown in the left panels of Fig. 5A-5I. In order to characterize the polarization on a broadband wavelength range, we have selected a Thorlabs mounted Superachromatic quarter waveplate (AQWP05M-600) with rotation angle of  $\theta_{\lambda/4} = 67.5^\circ$  and a broadband Thorlabs linear polarizer (WP25M-VIS) with rotation angle of  $\theta_{LP} = 49.07^\circ$  which were positioned between the meta-hologram and the projector to block the holographic images of designed SoP (details of setup are shown in the Supplementary fig. S11). With this choice of waveplate/polarizer orientations, holographic images are almost totally blocked in the entire visible range as shown in the right panels of Fig. 5A-5I, thus confirming the exceptional broadband response of our polarization-maintaining design approach. **The viewing angle of the holographic image is related to the operating wavelength as  $\Theta = 2\arcsin(\lambda / 2P_h)$ , where  $P_h$  is the pixel size of the hologram. Therefore, the blue holographic image has smaller size than the red holographic image.** To further quantify experimentally the SoP, we projected the holographic images into a broadband polarimeter which indicated that the SoP is correctly maintained around the designed value as shown in Fig. 5J. **Since the pixel size of the meta-hologram is larger than the operating wavelength, there are higher order images generated, which decrease the efficiency of the interested order as measured in Fig. 5K. It is possible to increase the efficiency by decreasing the pixel size to subwavelength scale. We have added a simulation proving that higher efficiency with subwavelength pixel size is achievable, referring to Supplementary fig. S6.** It should be noted that the unlimited bandwidth of polarization-maintaining behaviour is conserved for all of the input polarization (see details in Supplementary Note 2). The only limitation of our design approach concerns the addressing of arbitrary polarization state that are realized for all of the input polarization except for two pure input CP beams (see details in Supplementary Note 4).

### Angular nondispersive wavefront shaping using cascaded metasurface

According to Eq. S7 in the Supplementary, the deflection angle is in general subjected to the incident wavelength, i.e. in other words the deflection function of the device remains chromatically dispersive. However, such angle dependent dispersive response can be treated using appropriate combination of metasurfaces with refractive dispersive materials (40), which would resolve this issue (see more details in Supplementary Note 5). The idea to address chromatic angular dispersion is straightforward and consists in utilizing cascaded parallel metasurfaces, designed for  $\alpha = 0^\circ$  (see definition of  $\alpha$  in Supplementary Fig. S7A), as shown in Fig. 6A. Thus, the transmitted angle can be described from Eq. S27 as

$$\theta_t = \arcsin\left(\frac{\lambda\delta_d}{\pi P} + \frac{\lambda\delta'_d}{\pi P}\right) \quad (3)$$

It can be seen that when the increment rotation angle of the two metasurfaces are opposite ( $\delta_d = -\delta'_d$ ), i.e. when the angular dispersive properties of each metasurfaces compensate, a constant transmission angle  $\theta_t = 0^\circ$  is obtained, leading to a perfect angular

239 nondispersive metasurface with unlimited bandwidth and without any additional  
240 approximations as shown in Fig. 6B. The fabrication details and results are shown in  
241 Supplementary fig. S10. The same optical setup of fig. S11 is used here to capture the  
242 angular nondispersive holographic image, but the transmitted angle of the image is zero.  
243 The experimental results of the dispersive and nondispersive holographic images are  
244 shown in Fig. 6C and 6D, respectively Two spots observed at the exit of the doublet as  
245 shown in Fig. 6D are induced by the first layer of deflector as shown in the green light  
246 path in Fig. 6A (explaining the weaker intensity on right spot with respect to left  
247 counterpart). The holographic images are then projected at the entrance slit of a  
248 spectrometer to perform spectrum characterization at specific position along the image  
249 located at P1, P2, ... P5 (which is chosen from left edge to the right edge of the image) as  
250 shown in Fig. 6C and 6D. As it is expected for the dispersive case, the spectrum of the  
251 hologram red shift according to the angular dispersion law for larger deflection angles, as  
252 shown in Fig. 6E. Therefore, P1 has more intensity in the blue range, while P5 has more in  
253 the red range. Note that the relative intensities in P1 to P5 are changing due to the size of  
254 the actual portion of the image considered in the experiment. Comparatively, the  
255 nondispersive and polarization-maintaining case, all spectra always remain broadband at  
256 all the positions across the image as shown in Fig. 6F.

## 257 Discussion

259 In conclusion, we have demonstrated a general method of full-polarization generation and  
260 bandwidth unlimited polarization-maintaining diffractive planar optics. It relies on the  
261 superposition of orthogonal polarizations generated by PB phase metasurfaces composed  
262 of a unique element to eliminate the dispersive response of the structures. By linear  
263 superposition of amplitude-controlled polarization handedness, using RLL and LRR  
264 configurations, full polarization generation is established over an exceptionally unlimited  
265 bandwidth, experimentally demonstrated across the entire visible range from 475 nm to  
266 675 nm. The realization of a metasurface-doublet, involving an additional beam deflector  
267 with opposite deflection properties, is shown to address both the angular as well as the  
268 polarization chromatic dispersion over an extremely large bandwidth. The capability of  
269 generating and maintaining any arbitrary state of polarization on the entire visible range  
270 would lead to a plethora of promising applications in full color displays,  
271 augmented/virtual reality display, broadband polarization camera, vector beam generation  
272 and visible light communication, *etc.*

## 273 Materials and Methods

### 274 Device fabrication

277 The fabrication processes are shown in fig. S9 in the Supplementary. A Molecular Beam  
278 Epitaxy (MBE) RIBER system is used to grow GaN thin-film with 1  $\mu\text{m}$  thickness on a  
279 double-side polished *c*-plan sapphire substrate. The GaN nanopillars are patterned by  
280 using conventional electron beam lithography (EBL) processes. We spin coat  $\sim 180$  nm of  
281 PMMA resist (495A4) on the GaN thin-film and bake it on a hot plate at a temperature of  
282 125°C. The PMMA resist is exposed with designed patterns using electron beam  
283 lithography at 20 keV (Raith ElphyPlus, Zeiss Supra 40) and developed using 3:1  
284 IPA:MIBK solution. Subsequently, a 50 nm thick Ni is deposited on the sample using E-  
285 beam evaporation. After lift-off process by immersing the sample into acetone solution for  
286 2 hours, a Ni hard mask is obtained. The GaN nanorods is created by reactive ion etching

(RIE, Oxford system) with a plasma composed of  $\text{Cl}_2\text{CH}_4\text{Ar}$  gases. Followed by chemical etching with 1:1  $\text{H}_2\text{O}_2\text{:H}_2\text{SO}_4$  solution to remove the Ni hard mask, revealing a GaN nanopillar array.

## Optical setup

The optical setup for meta-hologram characterization is shown in Supplementary fig. S11. A laser beam propagates through a broadband linear polarizer (WP25M-VIS) with axis of transmission in horizontal direction to generate linear polarized input beam. It is weakly focused by an achromatic lens with a focal length of 50 mm onto the meta-hologram, which is mounted on a three-dimensional translation stage. The holographic image is projected onto a projector placed 10 cm away from the meta-hologram. A broadband quarter waveplate with fast axis at angle  $\theta_{\lambda/4}$  and a broadband linear polarizer with axis of transmission at angle  $\theta_{LP}$  are used to block selected images. Assume an incident beam  $\vec{E}_{in}$  propagates through the selected quarter waveplate and linear polarizer, the output electric field  $\vec{E}_{out}$  is described as  $\vec{E}_{out} = A_{LP}(\theta_{LP})A_{\lambda/4}(\theta_{\lambda/4})\vec{E}_{in}$ . Selected rotation angle  $\theta_{\lambda/4}$  and  $\theta_{LP}$  are chosen to block the specific output images (i.e.  $\vec{E}_{out} = \mathbf{0}$ ).

## H2: Supplementary Materials

Supplementary Materials for this article are available.

Note 1. Derivation of complex transmission of CP conversion.

Note 2. Unlimited bandwidth of polarization-maintaining with arbitrary input SoP.

Note 3. Evolution of the output SoP by changing the incident SoP with fixed configuration of metasurface.

Note 4. Full polarization generation with arbitrary fixed input SoP except two pure CP beams.

Note 5. Angular nondispersive design with prism.

Fig. S1. Schematic of the light path passing through the single layer metasurface.

Fig. S2. Output SoP of the metasurface with fixed configuration under arbitrary input SoP.

Fig. S3. Ellipticity angle as a function of  $a_+^0$  when  $0 < a_+^0 < 1$ .

Fig. S4. Output SoP of the metasurface under arbitrary input SoP.

Fig. S5. Simulation results of the 1- $\mu\text{m}$ -thick GaN nano-pillars on sapphire substrate with period of  $P = 300$  nm at the wavelength of 600 nm.

Fig. S6. Simulation results of the 1- $\mu\text{m}$ -thick GaN nano-pillars on sapphire substrate with the period of  $P = 150$  nm.

Fig. S7. Angular nondispersive design with prism.

Fig. S8. Simulated results with sapphire as the material of the prism.

Fig. S9. Fabrication processes of metasurface.

Fig. S10. Fabrication details of cascaded metasurfaces for angular nondispersive applications.

Fig. S11. Optical setup for the measurement of meta-hologram.

Table S1. SOA of the three lines and the corresponding ellipticity and azimuth angle of the four metasurfaces design in Figure 4.

## References and Notes

1. N. Yu, P. Genevet, M. A. Kats, F. Aieta, J.-P. Tetienne, F. Capasso, Z. Gaburro, Light Propagation with Phase Discontinuities: Generalized Laws of Reflection and Refraction. *Science* **334**, 333–337 (2011).
2. P. Genevet, F. Capasso, F. Aieta, M. Khorasaninejad, R. Devlin, Recent advances in planar optics: from plasmonic to dielectric metasurfaces. *Optica* **4**, 139 (2017).
3. G. Li, S. Zhang, T. Zentgraf, Nonlinear photonic metasurfaces. *Nat. Rev. Mater.* **2**, 17010 (2017).
4. Q. H. Song, W. M. Zhu, P. C. Wu, W. Zhang, Q. Y. S. Wu, J. H. Teng, Z. X. Shen, P. H. J. Chong, Q. X. Liang, Z. C. Yang, D. P. Tsai, T. Bourouina, Y. Leprince-Wang, A. Q. Liu, Liquid-metal-based metasurface for terahertz absorption material: Frequency-agile and wide-angle. *APL Mater.* **5**, 066103 (2017).
5. P. Genevet, D. Wintz, A. Ambrosio, A. She, R. Blanchard, F. Capasso, Controlled steering of Cherenkov surface plasmon wakes with a one-dimensional metamaterial. *Nat. Nanotechnol.* **10**, 804–809 (2015).
6. L. Yan, W. Zhu, M. F. Karim, H. Cai, A. Y. Gu, Z. Shen, P. H. J. Chong, D.-L. Kwong, C.-W. Qiu, A. Q. Liu, 0.2  $\lambda_0$  Thick Adaptive Retroreflector Made of Spin-Locked Metasurface. *Adv. Mater.* **30**, 1802721 (2018).
7. Q. H. Song, P. C. Wu, W. M. Zhu, W. Zhang, Z. X. Shen, P. H. J. Chong, Q. X. Liang, D. P. Tsai, T. Bourouina, Y. Leprince-Wang, A. Q. Liu, Split Archimedean spiral metasurface for controllable GHz asymmetric transmission. *Appl. Phys. Lett.* **114**, 151105 (2019).
8. J. Jang, H. Jeong, G. Hu, C.-W. Qiu, K. T. Nam, J. Rho, Kerker-Conditioned Dynamic Cryptographic Nanoprints. *Adv. Opt. Mater.* **7**, 1801070 (2019).
9. M. A. Ansari, I. Kim, D. Lee, M. H. Waseem, M. Zubair, N. Mahmood, T. Badloe, S. Yerci, T. Tauqeer, M. Q. Mehmood, J. Rho, A Spin-Encoded All-Dielectric Metahologram for Visible Light. *Laser Photonics Rev.* **13**, 1900065 (2019).
10. M. A. Ansari, I. Kim, I. D. Rukhlenko, M. Zubair, S. Yerci, T. Tauqeer, M. Q. Mehmood, J. Rho, Engineering spin and antiferromagnetic resonances to realize an efficient direction-multiplexed visible meta-hologram. *Nanoscale Horiz.* **5**, 57–64 (2019).
11. S. Wang, P. C. Wu, V.-C. Su, Y.-C. Lai, M.-K. Chen, H. Y. Kuo, B. H. Chen, Y. H. Chen, T.-T. Huang, J.-H. Wang, R.-M. Lin, C.-H. Kuan, T. Li, Z. Wang, S. Zhu, D. P. Tsai, A broadband achromatic metalens in the visible. *Nat. Nanotechnol.* **13**, 227–232 (2018).
12. J. Y. H. Teo, L. J. Wong, C. Molardi, P. Genevet, Controlling electromagnetic fields at boundaries of arbitrary geometries. *Phys. Rev. A* **94**, 023820 (2016).
13. A. Tittl, A. Leitis, M. Liu, F. Yesilkoy, D.-Y. Choi, D. N. Neshev, Y. S. Kivshar, H. Altug, Imaging-based molecular barcoding with pixelated dielectric metasurfaces. *Science* **360**, 1105–1109 (2018).
14. Y. Z. Shi, S. Xiong, Y. Zhang, L. K. Chin, Y. -Y. Chen, J. B. Zhang, T. H. Zhang, W. Ser, A. Larrison, S. H. Lim, J. H. Wu, T. N. Chen, Z. C. Yang, Y. L. Hao, B. Liedberg, P. H. Yap, K.

- 372 Wang, D. P. Tsai, C.-W. Qiu, A. Q. Liu, Sculpting nanoparticle dynamics for single-bacteria-  
373 level screening and direct binding-efficiency measurement. *Nat. Commun.* **9** (2018).
- 374 15. Q. Song, S. Khadir, S. Vézian, B. Damilano, P. de Mierry, S. Chenot, V. Brandli, R.  
375 Laberdesque, B. Wattellier, P. Genevet, Printing polarization and phase at the optical  
376 diffraction limit: near- and far-field optical encryption. *Nanophotonics* **1**, ahead-of-print  
377 (2020).
- 378 16. C. Pfeiffer, C. Zhang, V. Ray, L. J. Guo, A. Grbic, High performance bianisotropic  
379 metasurfaces: asymmetric transmission of light. *Phys. Rev. Lett.* **113**, 023902 (2014).
- 380 17. Y. Zhao, M. A. Belkin, A. Alù, Twisted optical metamaterials for planarized ultrathin  
381 broadband circular polarizers. *Nat. Commun.* **3** (2012).
- 382 18. N. Yu, F. Aieta, P. Genevet, M. A. Kats, Z. Gaburro, F. Capasso, A Broadband, Background-  
383 Free Quarter-Wave Plate Based on Plasmonic Metasurfaces. *Nano Lett.* **12**, 6328–6333  
384 (2012).
- 385 19. P. C. Wu, W.-Y. Tsai, W. T. Chen, Y.-W. Huang, T.-Y. Chen, J.-W. Chen, C. Y. Liao, C. H.  
386 Chu, G. Sun, D. P. Tsai, Versatile Polarization Generation with an Aluminum Plasmonic  
387 Metasurface. *Nano Lett.* **17**, 445–452 (2017).
- 388 20. Q. Song, A. Baroni, R. Sawant, P. Ni, V. Brandli, S. Chenot, S. Vézian, B. Damilano, P. de  
389 Mierry, S. Khadir, P. Ferrand, P. Genevet, Ptychography retrieval of fully polarized  
390 holograms from geometric-phase metasurfaces. *Nat. Commun.* **11** (2020).
- 391 21. P. Genevet, F. Capasso, Holographic optical metasurfaces: a review of current progress. *Rep.*  
392 *Prog. Phys.* **78**, 024401 (2015).
- 393 22. G. Zheng, H. Mühlenbernd, M. Kenney, G. Li, T. Zentgraf, S. Zhang, Metasurface holograms  
394 reaching 80% efficiency. *Nat. Nanotechnol.* **10**, 308–312 (2015).
- 395 23. H. Ren, G. Briere, X. Fang, P. Ni, R. Sawant, S. Héron, S. Chenot, S. Vézian, B. Damilano,  
396 V. Brändli, S. A. Maier, P. Genevet, Metasurface orbital angular momentum holography. *Nat.*  
397 *Commun.* **10** (2019).
- 398 24. Z.-L. Deng, J. Deng, X. Zhuang, S. Wang, T. Shi, G. P. Wang, Y. Wang, J. Xu, Y. Cao, X.  
399 Wang, X. Cheng, G. Li, X. Li, Facile metagrating holograms with broadband and extreme  
400 angle tolerance. *Light Sci. Appl.* **7** (2018).
- 401 25. L. Huang, S. Zhang, T. Zentgraf, Metasurface holography: from fundamentals to applications.  
402 *Nanophotonics* **7**, 1169–1190 (2018).
- 403 26. Y.-W. Huang, W. T. Chen, W.-Y. Tsai, P. C. Wu, C.-M. Wang, G. Sun, D. P. Tsai,  
404 Aluminum Plasmonic Multicolor Meta-Hologram. *Nano Lett.* **15**, 3122–3127 (2015).
- 405 27. Z.-L. Deng, G. Li, Metasurface optical holography. *Mater. Today Phys.* **3**, 16–32 (2017).
- 406 28. Z. Li, I. Kim, L. Zhang, M. Q. Mehmood, M. S. Anwar, M. Saleem, D. Lee, K. T. Nam, S.  
407 Zhang, B. Luk'yanchuk, Y. Wang, G. Zheng, J. Rho, C.-W. Qiu, Dielectric Meta-Holograms  
408 Enabled with Dual Magnetic Resonances in Visible Light. *ACS Nano* **11**, 9382–9389 (2017).

- 409 29. R. Zhao, B. Sain, Q. Wei, C. Tang, X. Li, T. Weiss, L. Huang, Y. Wang, T. Zentgraf,  
410 Multichannel vectorial holographic display and encryption. *Light Sci. Appl.* **7** (2018).
- 411 30. F. Dong, H. Feng, L. Xu, B. Wang, Z. Song, X. Zhang, L. Yan, X. Li, Y. Tian, W. Wang, L.  
412 Sun, Y. Li, W. Chu, Information Encoding with Optical Dielectric Metasurface via  
413 Independent Multichannels. *ACS Photonics* **6**, 230–237 (2019).
- 414 31. X. Zang, F. Dong, F. Yue, C. Zhang, L. Xu, Z. Song, M. Chen, P.-Y. Chen, G. S. Buller, Y.  
415 Zhu, S. Zhuang, W. Chu, S. Zhang, X. Chen, Polarization Encoded Color Image Embedded in  
416 a Dielectric Metasurface. *Adv. Mater.* **30**, 1707499 (2018).
- 417 32. F. Yue, D. Wen, J. Xin, B. D. Gerardot, J. Li, X. Chen, Vector Vortex Beam Generation with  
418 a Single Plasmonic Metasurface. *ACS Photonics* **3**, 1558–1563 (2016).
- 419 33. A. Shaltout, J. Liu, V. M. Shalaev, A. V. Kildishev, Optically Active Metasurface with Non-  
420 Chiral Plasmonic Nanoantennas. *Nano Lett.* **14**, 4426–4431 (2014).
- 421 34. Q. Guo, C. Schlickriede, D. Wang, H. Liu, Y. Xiang, T. Zentgraf, S. Zhang, Manipulation of  
422 vector beam polarization with geometric metasurfaces. *Opt. Express* **25**, 14300 (2017).
- 423 35. Z.-L. Deng, J. Deng, X. Zhuang, S. Wang, K. Li, Y. Wang, Y. Chi, X. Ye, J. Xu, G. P. Wang,  
424 R. Zhao, X. Wang, Y. Cao, X. Cheng, G. Li, X. Li, Diatomic Metasurface for Vectorial  
425 Holography. *Nano Lett.* **18**, 2885–2892 (2018).
- 426 36. Z. Deng, M. Jin, X. Ye, S. Wang, T. Shi, J. Deng, N. Mao, Y. Cao, B. Guan, A. Alù, G. Li, X.  
427 Li, Full- Color Complex- Amplitude Vectorial Holograms Based on Multi- Freedom  
428 Metasurfaces. *Adv. Funct. Mater.* 1910610 (2020).
- 429 37. A. Arbabi, Y. Horie, M. Bagheri, A. Faraon, Dielectric metasurfaces for complete control of  
430 phase and polarization with subwavelength spatial resolution and high transmission. *Nat.*  
431 *Nanotechnol.* **10**, 937–943 (2015).
- 432 38. E. Arbabi, S. M. Kamali, A. Arbabi, A. Faraon, Vectorial Holograms with a Dielectric  
433 Metasurface: Ultimate Polarization Pattern Generation. *ACS Photonics* **6**, 2712–2718 (2019).
- 434 39. J. P. Balthasar Mueller, N. A. Rubin, R. C. Devlin, B. Groever, F. Capasso, Metasurface  
435 Polarization Optics: Independent Phase Control of Arbitrary Orthogonal States of  
436 Polarization. *Phys. Rev. Lett.* **118** (2017).
- 437 40. R. Sawant, P. Bhumkar, A. Y. Zhu, P. Ni, F. Capasso, P. Genevet, Mitigating Chromatic  
438 Dispersion with Hybrid Optical Metasurfaces. *Adv. Mater.* 1805555 (2018).

439  
440

## 441 Acknowledgments

442

443 **Funding:** We acknowledge funding from the European Research Council (ERC) under  
444 the European Union’s Horizon 2020 research and innovation programme (Grant  
445 agreements no. 639109).

446

447 **Author contributions:** Q.S. and P.G. conceived the idea and carried out the experiment;  
448 Q.S. performed the numerical simulation and optical characterization of meta-hologram;

449 Q.S., S.C., and V.B. contributed to the nanofabrication. S.V., B.D., and P.D.M. performed  
450 the GaN MBE growth; Q.S., S.K., and P.G. wrote the manuscript; P.G. supervised and  
451 coordinated the project; all the authors discussed the results and approved the paper.

452 **Competing interests:** The authors declare that they have no competing interests.

453 **Data and materials availability:** All data needed to evaluate the conclusions in the paper  
454 are present in the paper and/or the Supplementary Materials. Additional data related to this  
455 paper may be requested from the corresponding author.  
456  
457  
458

## Caption of Figures

**Fig. 1. Linear superposition of circular polarization beams using phase gradient metasurfaces.** (A) A linear superposition of RCP and LCP with different size of meta-structures. (B) Schematic representation of the dispersive polarization response of the traditional polarization controlling metasurfaces. (C) Broadband polarization-maintaining design consisting in combination of RCP, LCP and LCP (or RCP, RCP and LCP) realized with a uniform size meta-structure. (D) Schematic representation of the broadband polarization-maintaining metasurfaces. (E) Angular nondispersive design with metasurface-doublet. (F) Schematic representation of the angular nondispersive metasurfaces.

**Fig. 2. Numerical simulation of the metasurfaces.** (A) Top view and (B) perspective view of one meta-structure.  $P = 300$  nm and  $h = 1000$  nm. (C) Simulated results of the polarization conversion efficiency  $a(\lambda)$  (red and black lines) and propagation phase  $\varphi(\lambda)$  (blue and green lines) with two different size of GaN nanopillars. Red and blue curves:  $L_{u1} = 170$  nm,  $L_{v1} = 70$  nm. Black and green curves:  $L_{u2} = 220$  nm,  $L_{v2} = 120$  nm. (D) Calculated azimuth angle and ellipticity angle of the output polarization and (E) the corresponding SoP on Poincaré sphere as a function of incident wavelength from 475 nm to 675 nm with dispersive superposition consisting of two different size of GaN nanopillars with zero SOA, indicating that the traditional linear superposition of opposite polarization leads to dispersive polarization response. (F) Calculated azimuth and ellipticity angles of the output polarization and (G) the corresponding SoP on Poincaré sphere as a function of incident wavelength from 475 nm to 675 nm with the proposed nondispersive superposition consisting of uniform size of GaN nanopillars with  $L_{u2} = 220$  nm,  $L_{v2} = 120$  nm,  $\delta_{L1} = 0^\circ$ ,  $\delta_{R1} = 22.5^\circ$ , and  $\delta_{R2} = 22.5^\circ$ , indicating that an assembly of a generic building block could realize broadband polarization-maintaining behavior with unlimited bandwidth.

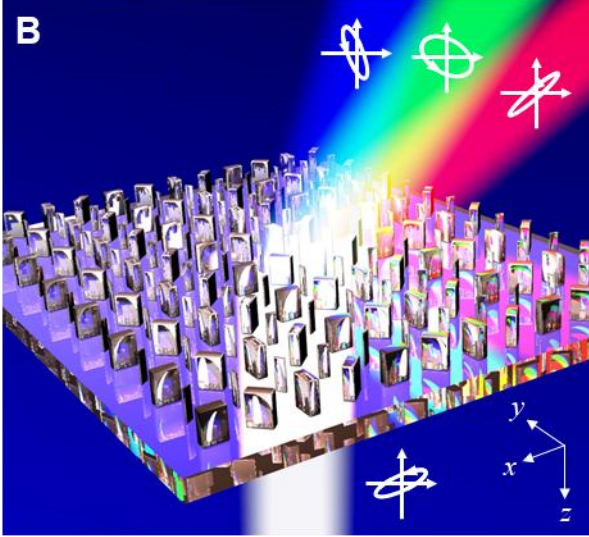
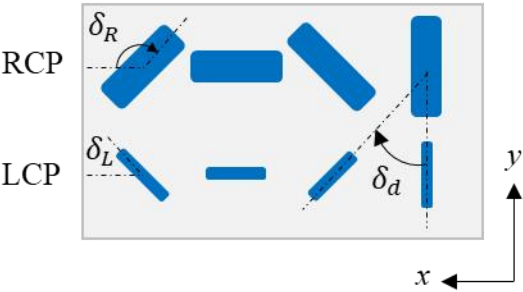
**Fig. 3. Design of full-polarization pixels using geometric-phase metasurface.** (A) One supercell of the metasurface consists of one LCP and two RCP beams. (B) Ellipticity angle and (C) azimuth angle of the output light as a function of rotation angle  $\delta_{R2}$  for fixed  $\delta_{L1} = 0^\circ$ . Black curve:  $\delta_{R1} = 0^\circ$ , red curve:  $\delta_{R1} = 30^\circ$ , blue curve:  $\delta_{R1} = 60^\circ$ . The corresponding Poincaré sphere when (D)  $\delta_{R1} = 0^\circ$ , (E)  $\delta_{R1} = 30^\circ$  and (F)  $\delta_{R1} = 60^\circ$ . (G) By controlling both  $\delta_{R1}$  and  $\delta_{R2}$  from  $0^\circ$  to  $180^\circ$ , the SoP covers the bottom sphere cap of Poincaré sphere with  $-\frac{\pi}{4} \leq \chi \leq \frac{1}{2} \arcsin \frac{3}{5}$ . (H) One supercell of metasurface consists of one RCP and two LCP beams. (I) Ellipticity angle and (J) orientation angle of the output light as a function of rotation angle  $\delta_{L2}$  for fixed  $\delta_{R1} = 0^\circ$ . Black curve:  $\delta_{R1} = 0^\circ$ , red curve:  $\delta_{R1} = 30^\circ$ , blue curve:  $\delta_{R1} = 60^\circ$ . The corresponding Poincaré sphere when (K)  $\delta_{R1} = 0^\circ$ , (L)  $\delta_{R1} = 30^\circ$  and (M)  $\delta_{R1} = 60^\circ$ . (N) By controlling both  $\delta_{L1}$  and  $\delta_{L2}$  from  $0^\circ$  to  $180^\circ$ , the SoP covers the top sphere cap of Poincaré sphere with  $-\frac{1}{2} \arcsin \frac{3}{5} \leq \chi \leq \frac{\pi}{4}$ . (G) and (N) indicate that the superposition of circular polarizations diffracted by array of a generic PB building block could produce any arbitrary SoP, without having to carefully engineers the meta-structure geometry for the desired application.

505  
506 **Fig. 4. Full-polarized meta-hologram.** (A) Top view and (B) tilt view of the SEM  
507 images of the metasurfaces. The red rectangular highlight area in A shows one  
508 pixel of the meta-holograms. (C) Measured holographic images (illumination at  $\lambda$   
509 = 600 nm.) of the meta-holograms. (D) Measured SoP on Poincaré sphere. Red  
510 dots: designed value, blue dots: measured value. (The scale bar in A and B is 1  
511  $\mu\text{m}$ ).

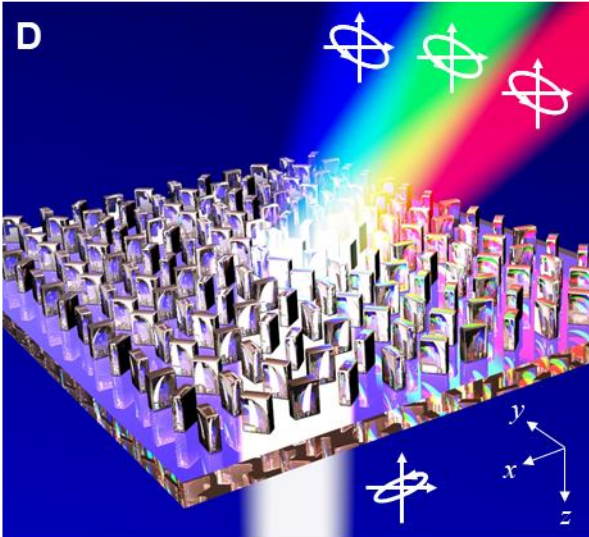
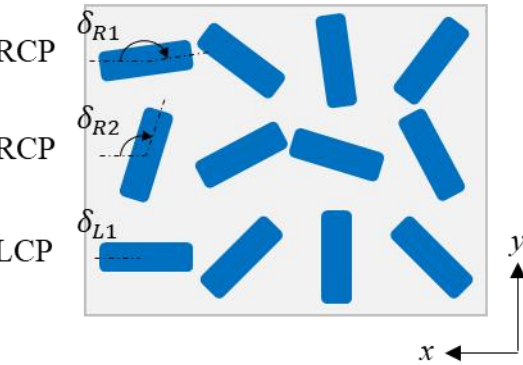
512  
513 **Fig. 5. Broadband polarization-maintaining properties of the nondispersive**  
514 **metasurface.** (A) - (I) Measured holographic images with the incident wavelength  
515 from 475 nm to 675 nm (Left panel: without analyser. Right panel: with broadband  
516 quarter waveplate at  $\theta_{\lambda/4} = 67.5^\circ$  and LP at  $\theta_{LP} = 49.07^\circ$  to block the holographic  
517 images). The holographic images in the right panels are almost totally blocked in  
518 the entire visible range, confirming the exceptional broadband response of out  
519 polarization-maintaining design approach. (J) Measured SoP at different  
520 wavelength agree well to the designed value in Fig. 2(G). (K) Measured efficiency  
521 is higher than 10% across the entire visible range.  
522

523 **Fig. 6. Angular nondispersive wavefront shaping using cascaded metasurface-**  
524 **doublet.** (A) Schematic of angular nondispersive design using two layers of  
525 metasurfaces on both sides of a sapphire substrate. The phase gradient of the two-  
526 layer metasurfaces are  $\frac{d\phi'}{dx'} = \frac{2\delta'_d}{P}$  on the top and  $\frac{d\phi}{dx} = \frac{2\delta_d}{P}$  on the bottom with  
527  $\delta_d = -\delta'_d = 30^\circ$ . A linearly broadband light is normally illuminated from the top  
528 metasurface and diffracted to the bottom metasurface. **Two spots are generated**  
529 **from the top deflector as shown in the green optical path.** (B) Transmitted angle  
530 with single layer metasurface (red curve) and double layer metasurfaces (blue  
531 curve). A nondispersive angle response is realized in unlimited bandwidth using  
532 double layer metasurfaces. Measurement results of the holographic image of  
533 “Spade” using (C) single layer metasurface and (D) double layer metasurfaces.  
534 The holograms are imaged at the entrance slit of a spectrometer for spectrum  
535 characterization. A slit with 20- $\mu\text{m}$ -width is placed to select a line of the image  
536 light at specific position of P1, P2, ... P5. The corresponding spectra for (E)  
537 dispersive case and (F) nondispersive case at position P1~P5, show a red-shift of  
538 the bandwidth for large angle in (E) while (F) spectrum are essentially broadband.  
539

**A**



**C**



**E**

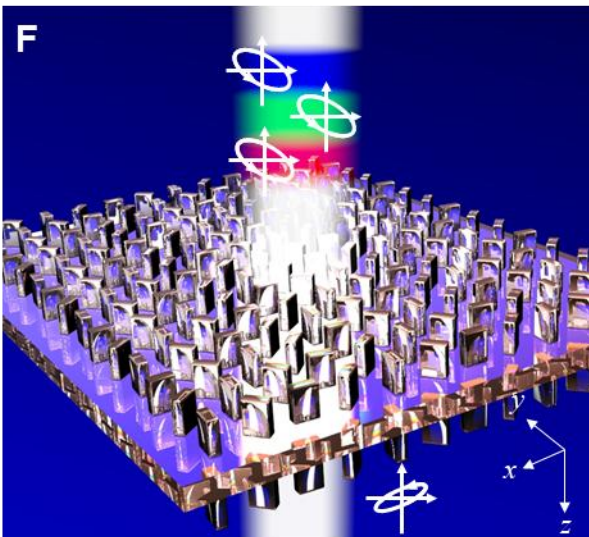
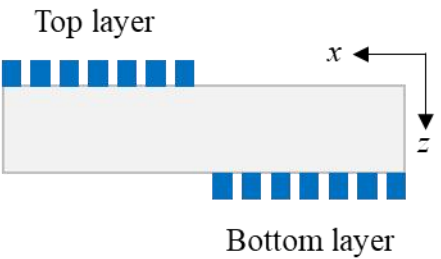


**Figure 1**

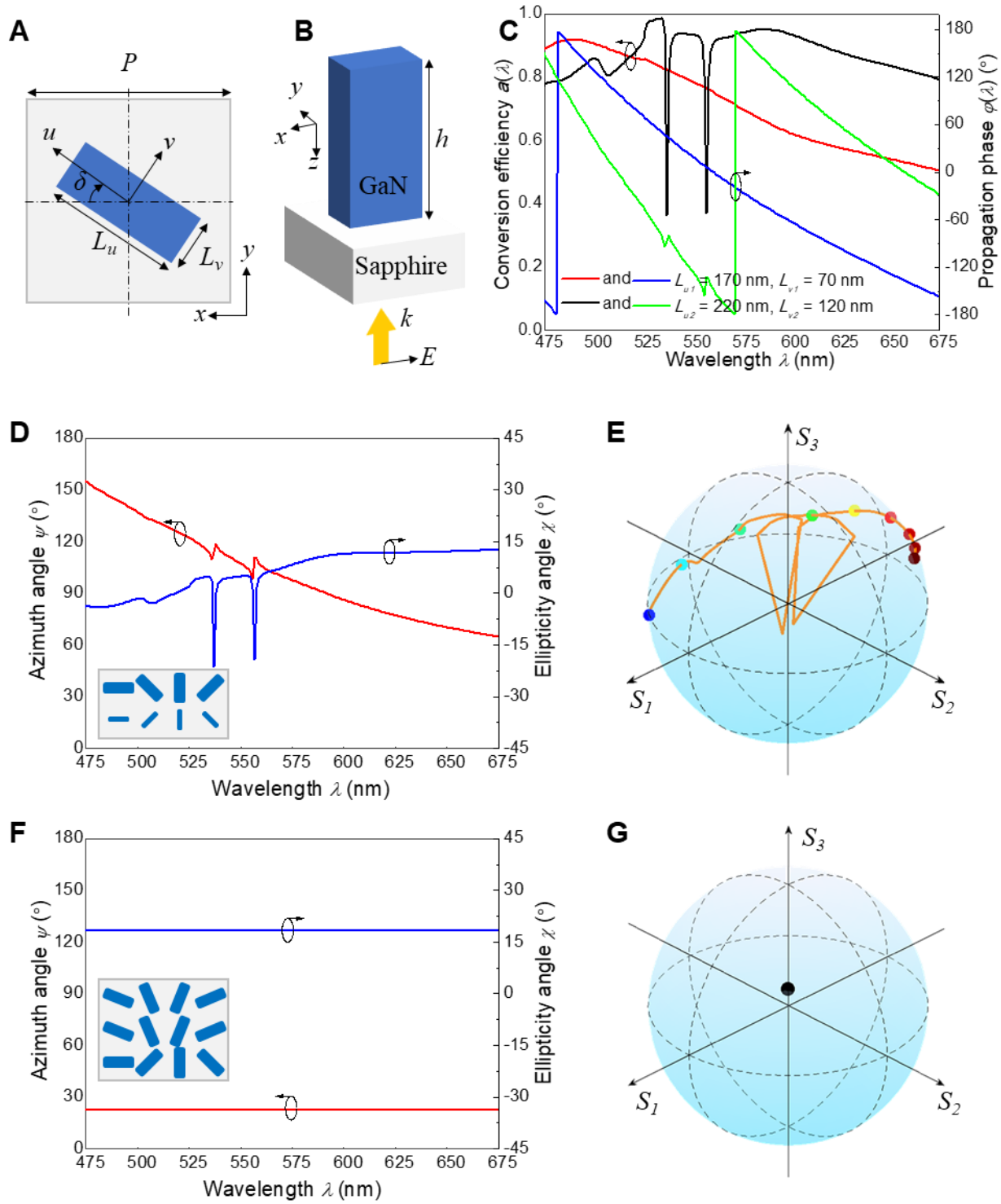


**Figure 2**

545  
546  
547

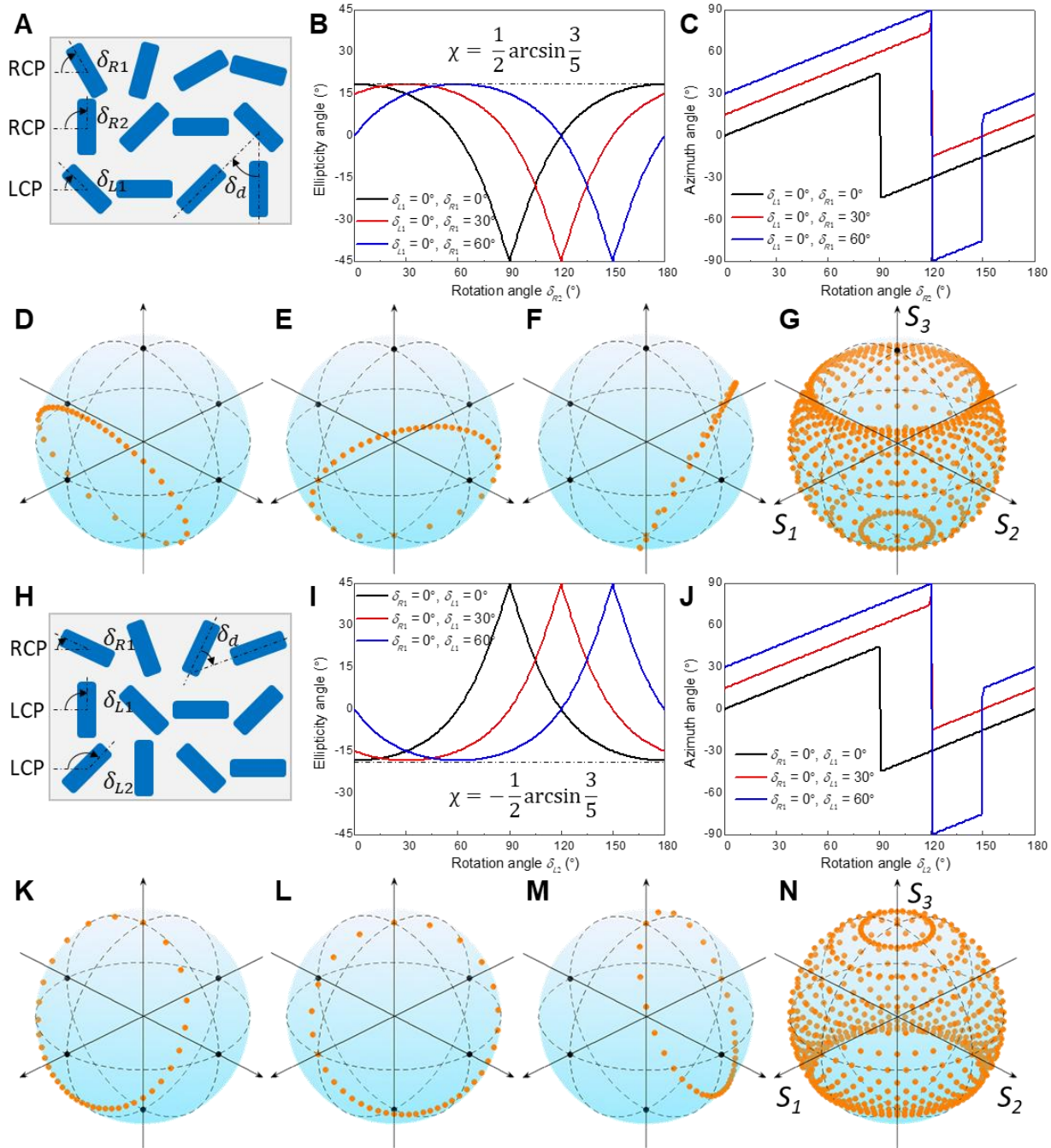


**Figure 3**

548  
549  
550

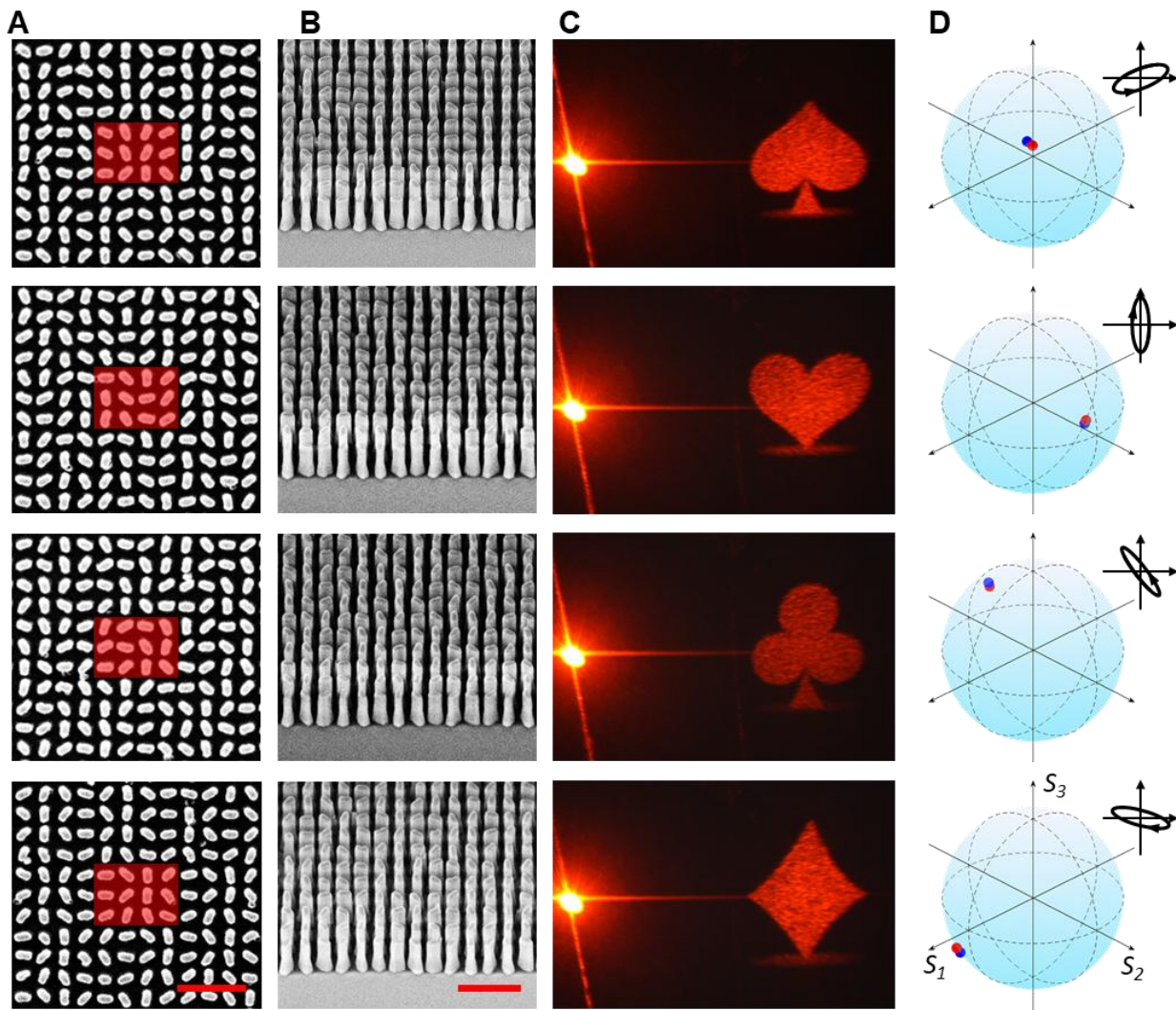
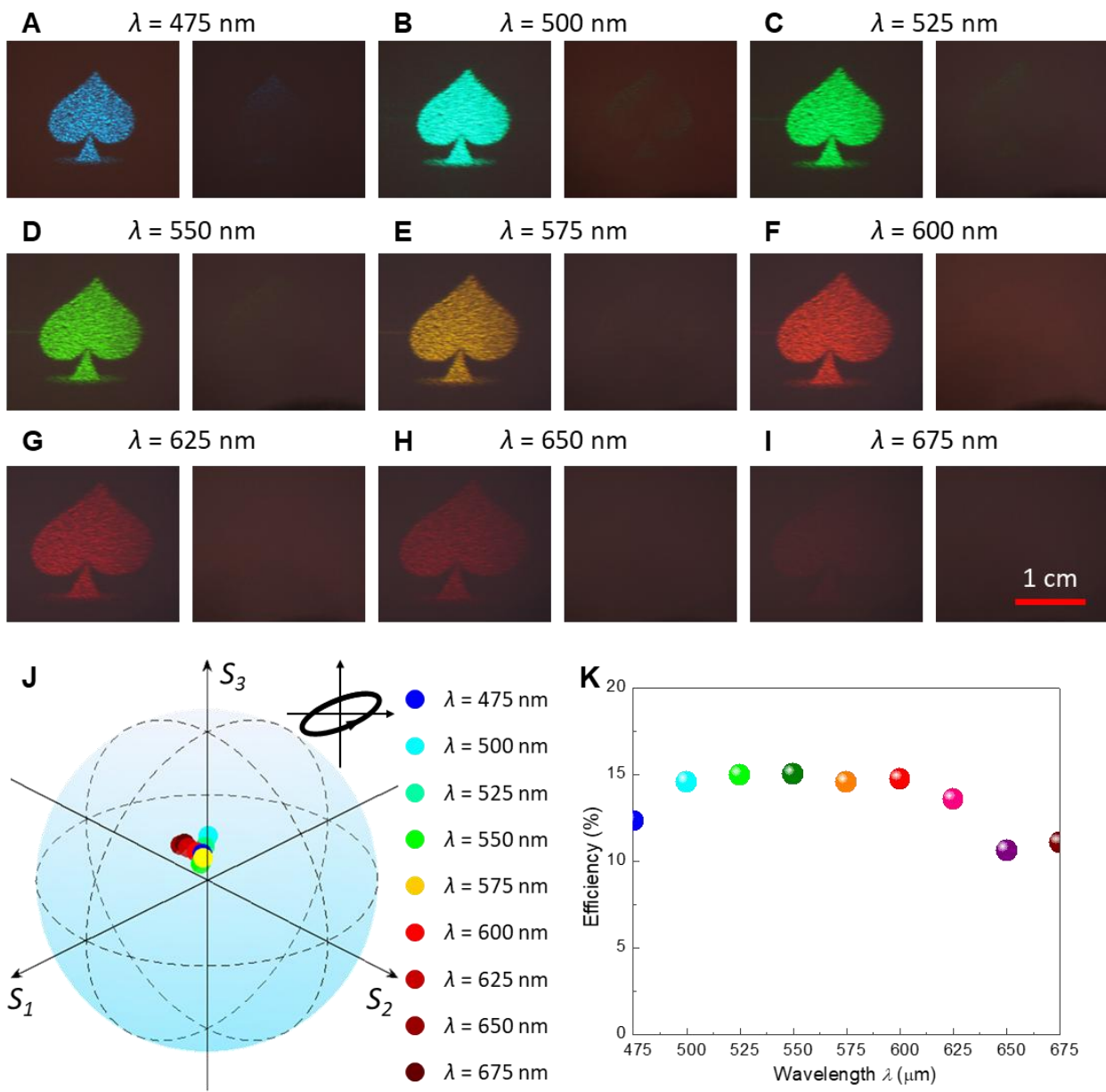


Figure 4

551  
552  
553



**Figure 5**

554  
555  
556

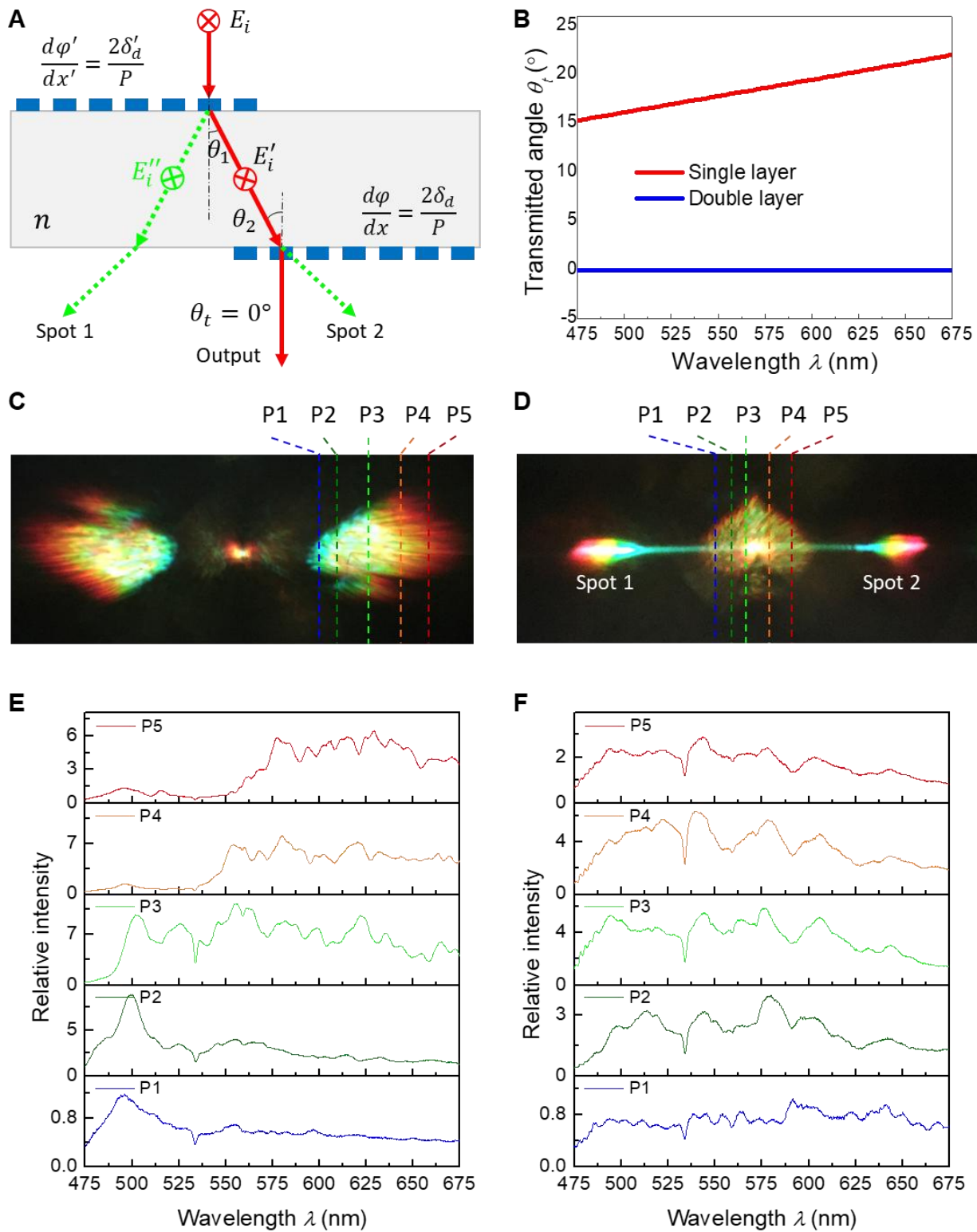


**Figure 6**

557  
558  
559

560 **Supplementary Materials**

561 Include the text, figures, and tables of the Supplementary Materials at the end of your  
562 Word manuscript if possible. Include captions for other file types (see below).